Supplementary Information

Multi-layered stochasticity and paracrine signal propagation shape the type-I interferon response

Ulfert Rand, Melanie Rinas, Johannes Schwerk, Gesa Nöhren, Melanie Linnes, Andrea Kröger, Michael Flossdorf, Kristóf Kály-Kullai, Hansjörg Hauser, Thomas Höfer, and Mario Köster

Table of contents

MATLAB codes for all model simulations are available as separate suppl. files

Supplementary Figures

Figure S1

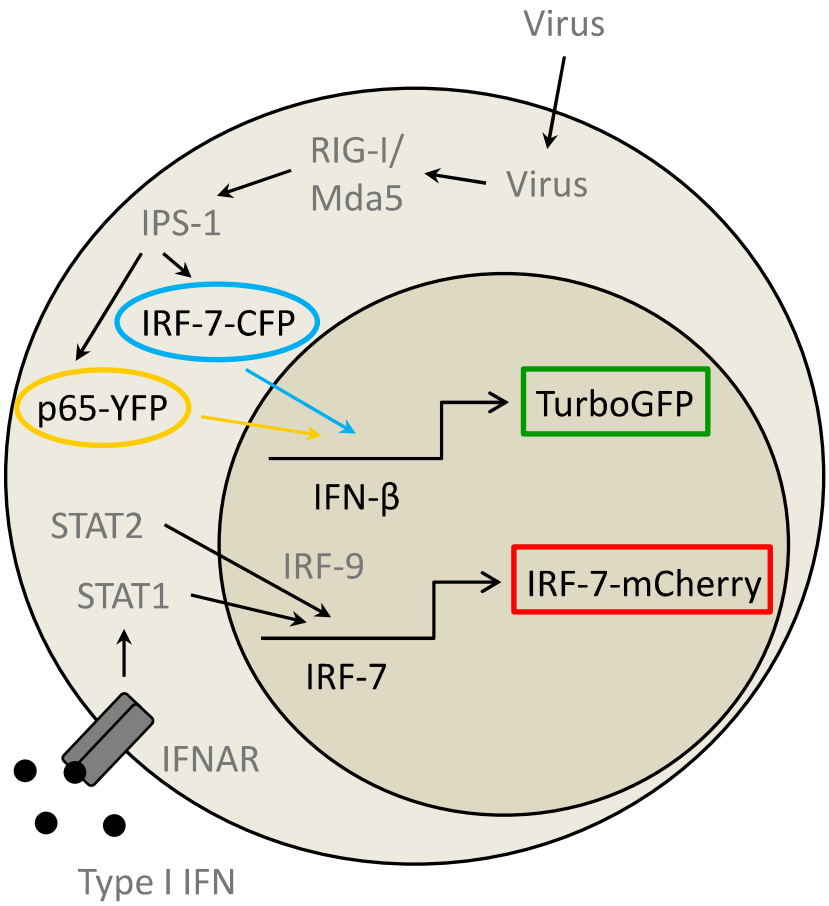

Figure S1 | Intracellular reporters.
Nuclear translocation of the fusion proteins IRF-7-CFP and NF-κB/p65-YFP represent activation of signal transduction following virus recognition by RIG-I/Mda5. The BAC reporter IFN-β-tGFP contains TurboGFP under control of the murine IFN-β promoter and flanking regions. Within the BAC construct IRF-7-mCherry the mCherry gene is linked to the C-terminal end of the genomic IRF-7 sequence resulting in a fusion protein. The complete intron-exon organization of IRF-7 keeps intact. All reporter constructs were transfected into NIH3T3 cells and representative stable cell clones were used for the studies.

Figure S2

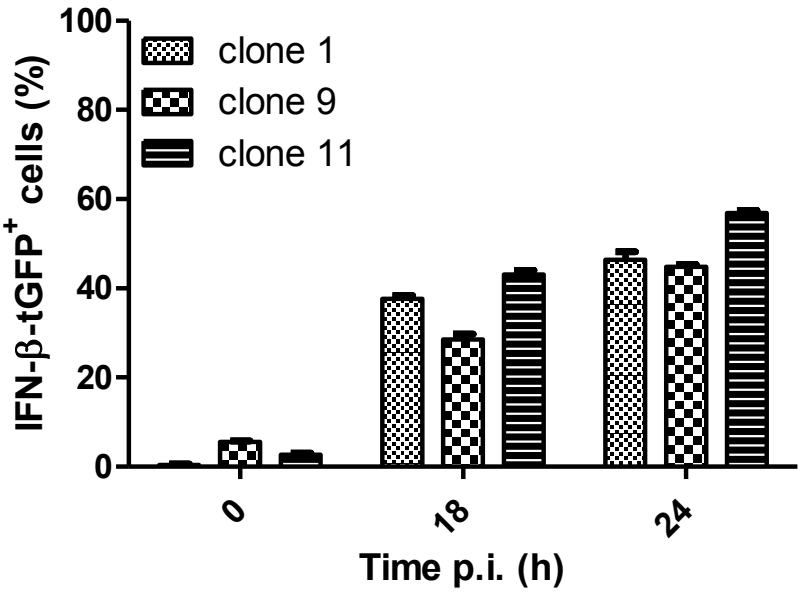

Figure S2 | Stochastic IFN-β-tGFP expression in different cell clones.
NIH3T3 cell clones expressing IFN-β-tGFP (10^5 cells/ml) were infected with 80 HAU/ml NDV for one hour or left untreated. Flow cytometry for TurboGFP expression was performed 18h and 24h after stimulation. Frequencies of expression (mean, +/- SD) are shown.

Figure S3

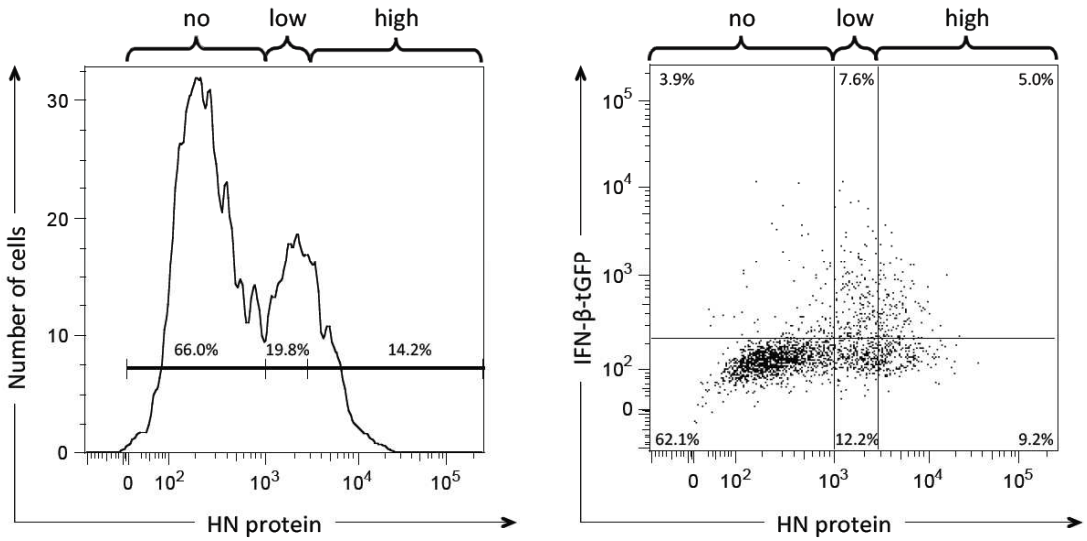

Figure S3 | Extent of NDV replication and frequency of IFN-β-tGFP expressing cells. NIH3T3 cells stably expressing the BAC construct IFN-β-tGFP were infected with 40 HAU/ml NDV for 1 hour. After 24 hours IFN-β-tGFP reporter expression and intracellular NDV HN protein were detected by flow cytometry. The bimodal behaviour of HN intensity clearly shows a subdivision between cells with replicating virus (left diagram). We divided the infected cells into three fractions with respect to HN-expression. The subpopulations expressing low and high HN protein contain nearly the same fraction of tGFP-positive cells (38% and 36%, respectively). By comparison, the fraction of tGFP-positive cells in the HN-negative population is negligible (6%) (right diagram).

Figure S4

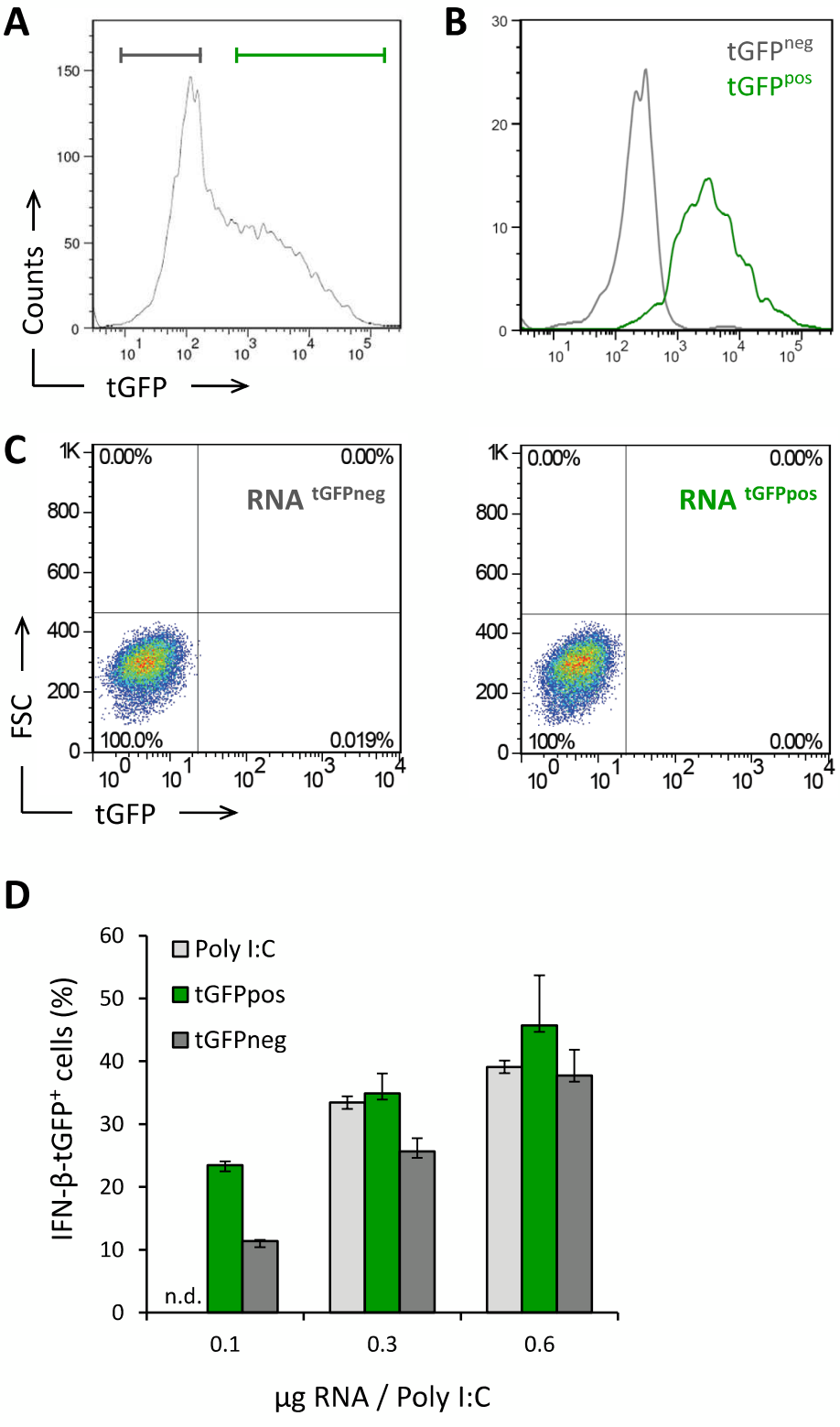
A
Counts
tGFP
B
tGFPneg
tGFPpos
C
RNA tGFPneg
RNA tGFPpos
FSC
tGFP
0.00%
100.0%
0.019%
100%
D
Poly I:C
tGFPpos
tGFPneg
IFN-β-tGFP+ cells (%)
n.d.
0.1
0.3
0.6
µg RNA / Poly I:C

Figure S4 | Induction of IFN-β by RNA from fractions of infected cells expressing or not expressing IFN-β-tGFP.
(A) NIH3T3 cells stably expressing the BAC construct IFN-β-tGFP were infected with 80 HAU/ml NDV for one hour. After 20 hours tGFP positive (green marker line) and negative (grey marker line) populations were separated by fluorescence activated cell sorting. **(B)** Sorted cell populations were re-analyzed by flow cytometry for tGFP expression. **(C)** Total RNA was prepared from both populations. To exclude that total RNA of the tGFP positive cell population contains sufficient amounts of preexisting mRNA encoding for tGFP RNA from both populations were transfected into w.t. NIH3T3 cells using Lipofectamine 2000. 24 hours after transfection cells were analyzed by flow cytometry. **(D)** The indicated amounts of total RNA from tGFP positive (green bars) and negative (grey bars) populations were transfected into IFN-β-tGFP reporter cells. 24 hours after transfection cells were analyzed by flow cytometry for induction of the IFN-β promoter. Poly I:C was used as a control (light grey bars).

Figure S5

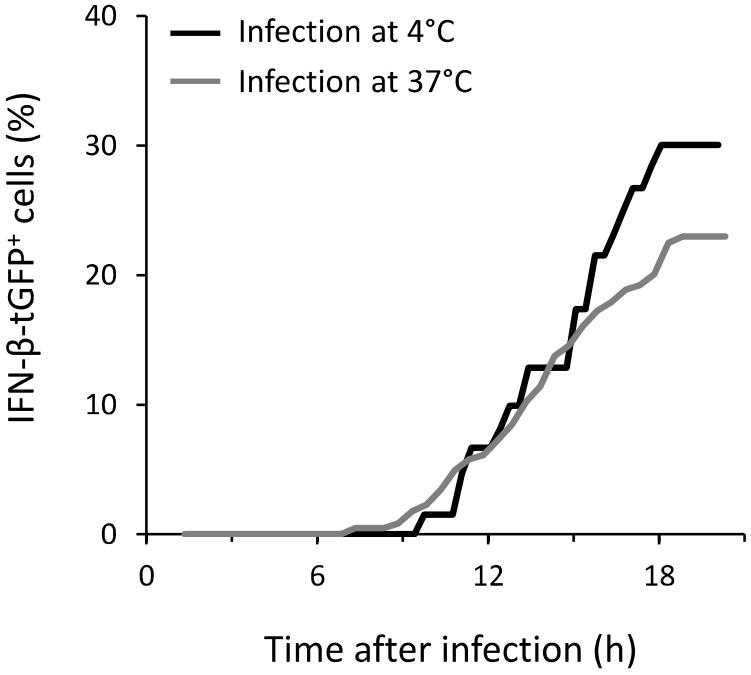

Figure S5 | Increase of IFN-β-tGFP expressing cells over time after NDV synchronised infection.
NIH3T3 cells stably expressing the BAC construct IFN-β-tGFP were infected with 80 HAU/ml NDV for one hour at 4°C (black line) and 37°C (grey line). Cells were extensively washed with cold or pre-warmed medium, respectively, pre-warmed medium was added to both cultures and cells were subjected to time-lapse microcopy in a 37°C incubation chamber. Pictures were taken every 20 minutes. The onset time points for IFN-β-tGFP expression in individual cells were determined at each time frame and the increase in the total number of tGFP-positive cells was plotted over time.

Figure S6

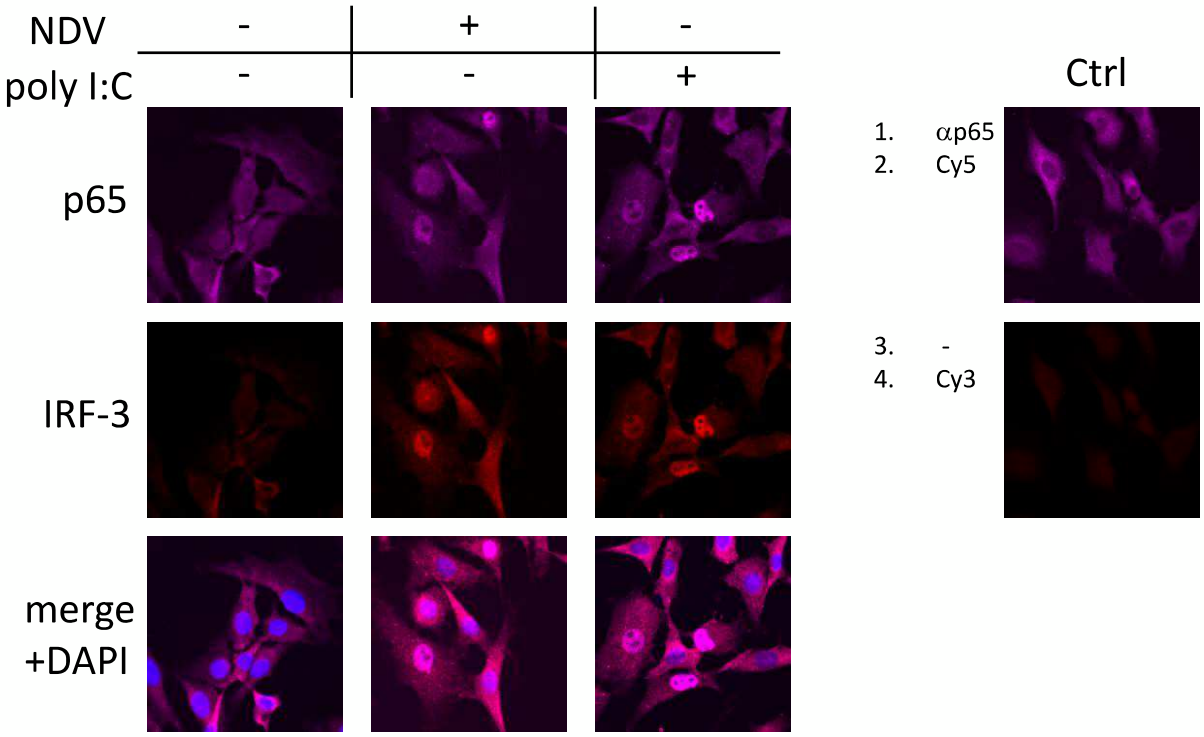

Figure S6 | Synchronous nuclear translocation of endogenous IRF-3 and NF-κB. NIH3T3 cells were seeded on cover slips (10^5 cells/ml) and infected with NDV (80 HAU/ml), transfected with poly I:C (5µg/ml) or left untreated. After 8h, cells were fixed and immunofluorescent staining was performed for the endogenously expressed p65 subunit of NF-κB and for IRF-3. Nuclei were stained with DAPI. As both primary antibodies were raised in rabbits staining control was done to check that blocking prevents cross-staining of secondary antibody (right panel).

Figure S7

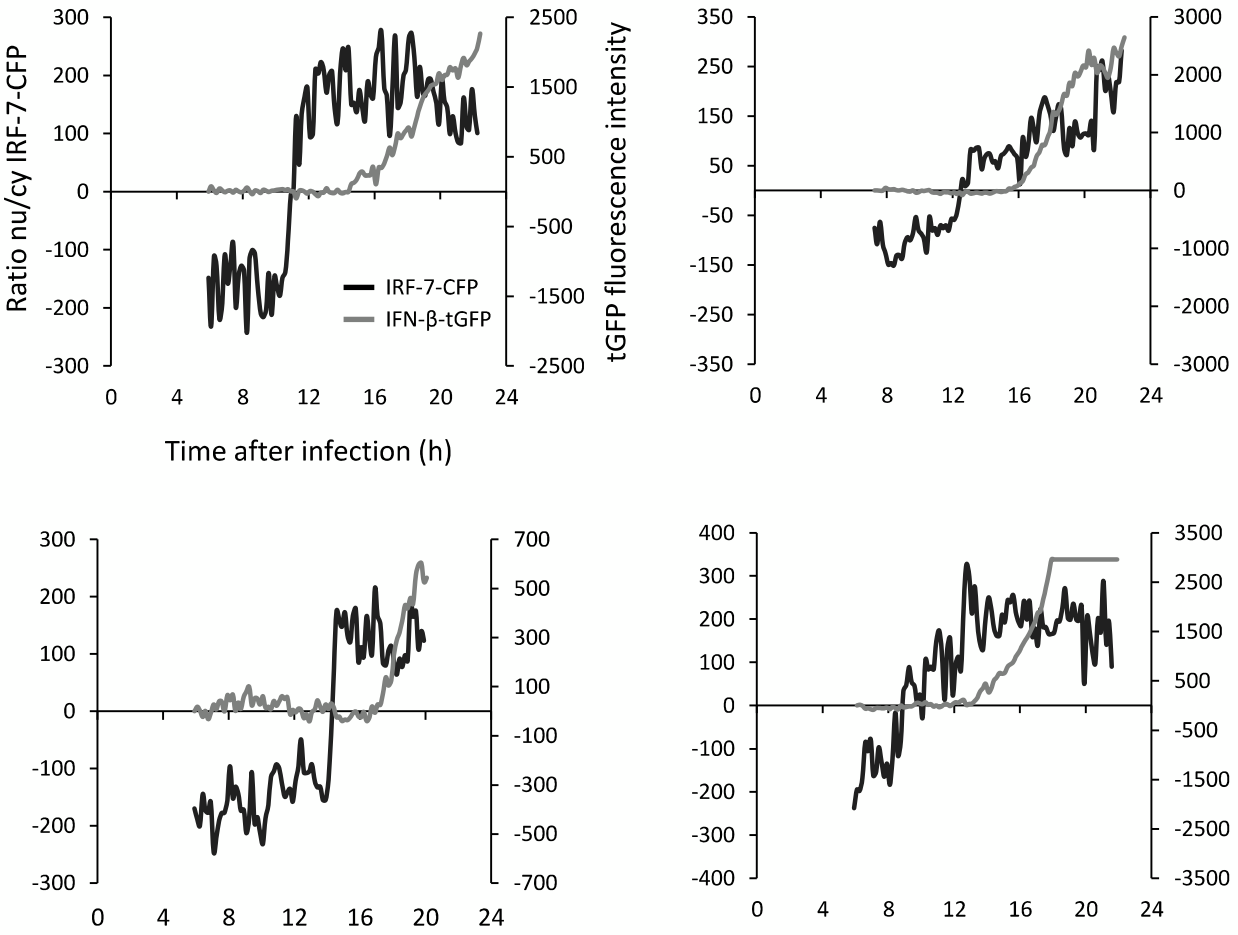

Figure S7 | Kinetics of IRF-7 nuclear translocation and IFN-β-tGFP expression within individual cells.
NIH3T3 cells stably expressing IFN-β-tGFP and IRF-7-CFP fusion protein were infected with 80 HAU/ml NDV for 1 hour. Cells were subjected to time-lapse microscopy and fluorescent pictures were taken every 30 minutes. The ratio of nuclear to cytoplasmic IRF-7-CFP fluorescence intensity as well as the overall intensity of IFN-β-tGFP was quantified using ImageJ plugin MtrackJ. Four representative intensity courses of single cells are depicted. Black lines show the nuclear to cytoplasmic ratio of IRF-7-CFP fluorescence, grey lines represent IFN-β-tGFP fluorescence.

Figure S8

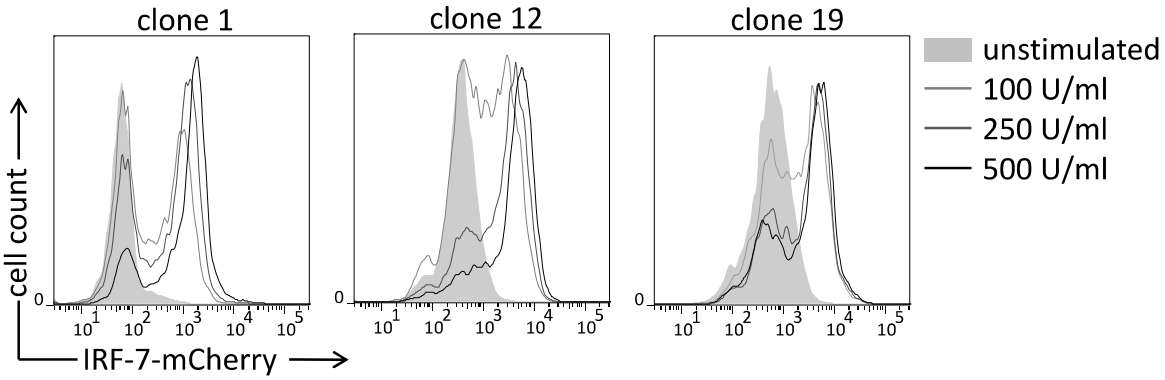

Figure S8 | Stochastic bimodal IRF-7-mCherry expression in different cell clones. 100, 250 or 500 U/ml IFN-β were added to NIH3T3 IRF-7-mCherry cells (10^5 cells/ml) of clones 1, 12 and 19. Flow cytometry for mCherry expression was performed 24h after stimulation.

Figure S9

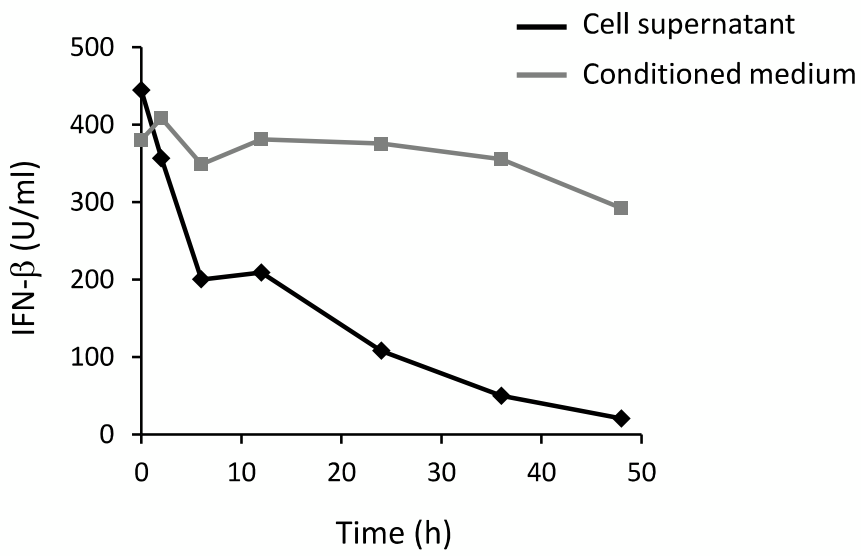

Figure S9 | Kinetics of IFN-β activity disappearance in the supernatant of cells.
500 U/ml IFN-β was added to NIH3T3 cells (10^5 cells/ml). At different time points supernatant (black diamonds) was collected and type I IFN concentration was determined in the medium by using Mx2-Luc cell-based assay (Kugel *et al.*, 2010). IFN stability in conditioned medium at 37°C was measured in parallel (grey squares).

Figure S10

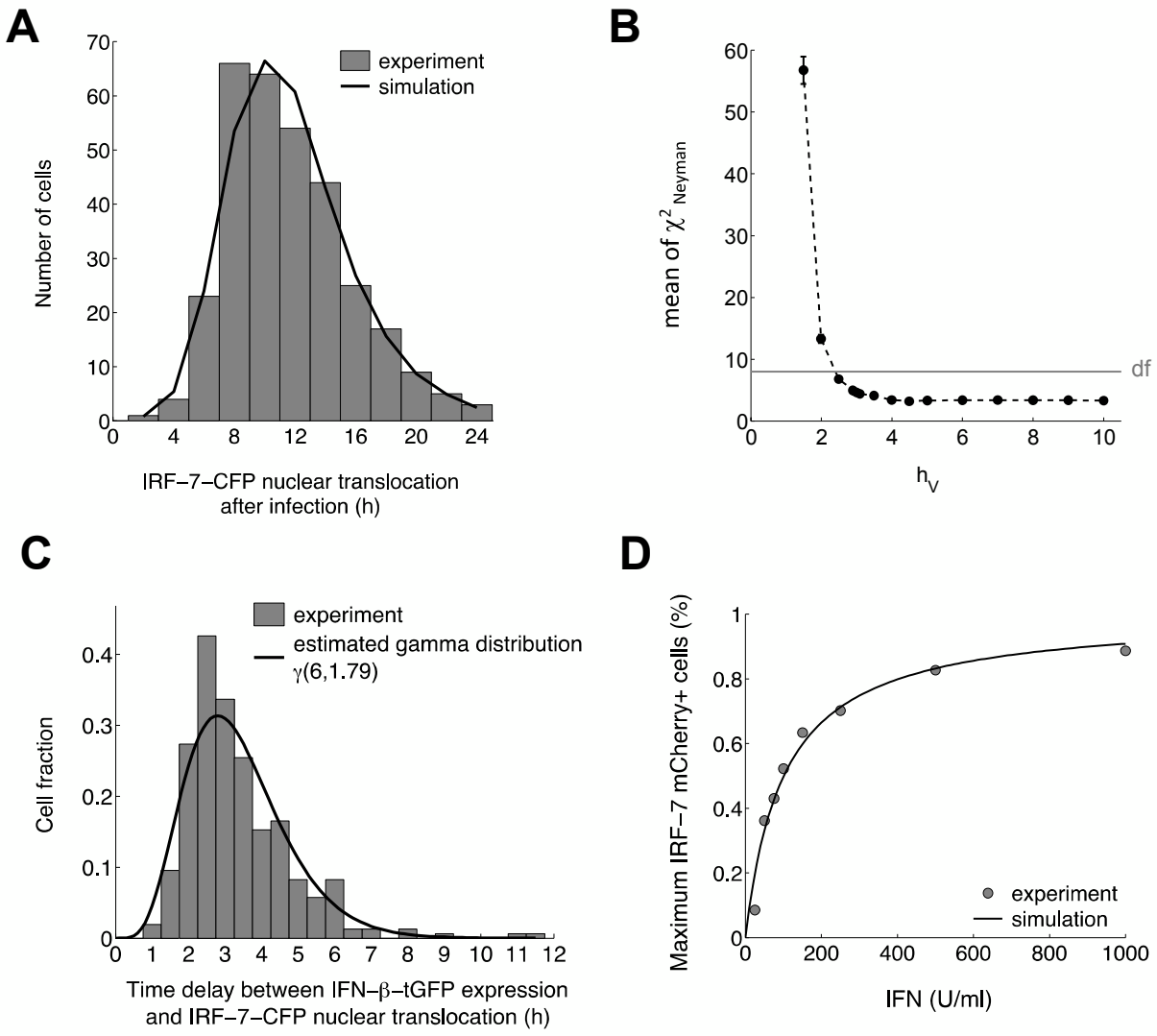

Figure S10 | Parameter estimation for the stochastic model.
(A) Bar diagram: Experimentally measured distribution of IRF-7-CFP nuclear translocation times after NDV infection (80 HAU/ml); Solid line: Distribution obtained by simulating $5x10^4$ runs of the mathematical model. The model parameters were fitted as described in Supplementary Text S1. **(B)** Profile likelihood with respect to the Hill coefficient of virus-induced RIG-I signalling, h_V. Shown are the mean χ^2_{Neyman} values obtained by simulating 10^4 runs of the stochastic model with the respective optimized parameter sets. For good fits, χ^2_{Neyman} is of the order of the degrees of freedom (df = # histogram bins - 1 - # fit parameters = 8). **(C)** Bar diagram: Measured distribution of the time delay from IRF-7-CFP nuclear translocation to onset of IFN-β-tGFP fluorescence. Solid line: Fit by a Gamma distribution. For details see Supplementary Text S1. **(D)** Dots: Measured fraction of IRF-7-mCherry positive cells; primary data are shown in Figure 5A, the maximum over the time course is plotted for each IFN-β concentration. Solid line: Fit of the data by Michaelis-Menten-type function (Supplementary Text S1).

Figure S11

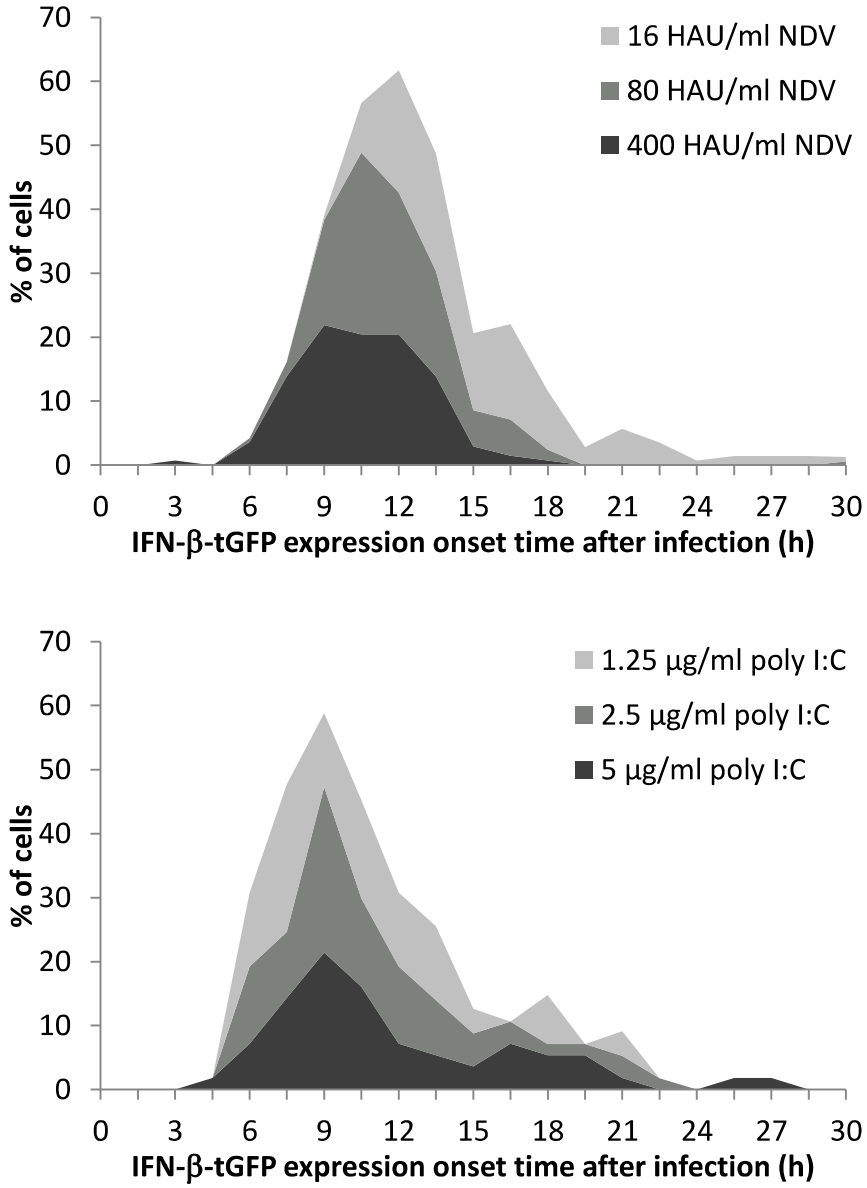

Figure S11 | Temporal distribution of cellular IFN-β induction.
NIH3T3 IFN-β-tGFP reporter cells infected for 1 hour with indicated concentrations of NDV (upper panel) or transfected with poly I:C at given concentrations (lower panel) were subjected to time-lapse microscopy (15 min picture intervals) (cf. Figure 3A). Distribution of tGFP expression onset over time following NDV infection (n = 456) or following poly I:C lipofection (n = 140) is shown as histograms with 1.5 h bins.

Supplementary Movies

Movie S1
This movie shows IFN-β-tGFP reporter cells infected with NDV (80 HAU/ml) in a time lapse of 20 h (pictures taken every 0.5 h). Temporal and quantitative heterogeneity of IFN-β expression becomes evident by following the cells. (MPG format; 2.0 MB)

Movie S2
The movie presents IRF-7-mCherry cells upon stimulation with IFN-β (500 U/ml). This clip covers about 50 h with pictures taken every 0.5 h. The kinetics of IRF-7 expression resulting from IFN-β treatment within individual cells become obvious. (MPG format; 2.7 MB)

Supplementary Modeling Files

These modeling files are available online:

Model_Figure_6
Comparison_model_experiment_Figure_7A
Paracrine_amplification_Figure_7B
Parameter_estimation_NFkB_IRF_activation_Figure_S10_A_B
Parameter_estimation_IFNb_expression_Figure_S10_C
Parameter_estimation_ISG_induction_Figure_S10_D

All files are written in MATLAB.

Supplementary Table

Table S1 | Model parameters

Model parameter	Symbol	Value
Maximum viral load per cell	V_{max}	130
Rate constant of virus replication	r	0.34/h
Rate constant of virus decay	d	0.1/h
Rate of RIG-I pathway stimulation	$k_{RIG\text{-}I}$	0.48/h
Rate of RIG-I pathway inactivation	$l_{RIG\text{-}I}$	0.4/h
Half-saturation constant of RIG-I pathway stimulation by virus	K_V	43
Hill coefficient of RIG-I pathway stimulation by virus	h_V	3
Rate constant of IFN-β induction	k_{IFN}	1.79/h
Rate of termination of IFN-β expression	l_{IFN}	0.08/h
Rate constant of IFN-β secretion	k_S	0.13 U/(h ml cell)
Rate constant of IFN-β degradation	d_{IFN}	0.15/h
Rate constant of STAT1/2 pathway activation	k_{STAT}	0.1/h
Half-saturation constant of STAT1/2 pathway activation by IFN-β	K_{IFN}	100 U/ml
Hill coefficient of STAT1/2 pathway activation by IFN-β	h_{IFN}	1
Rate constant of ISG (IRF-7) induction by STAT1/2 pathway	k_{ISG}	0.1/h

Supplementary Text

Text S1 | Mathematical Modelling

1. Model description

To describe the stochastic dynamics of the IFN network we developed a multi-scale model for an ensemble of N cells communicating via secreted IFN-β. The stochastic transitions of the cells with respect to virus replication, IFN-β induction and ISG expression (Figure 6A) were iterated using Gillespie's algorithm. The extracellular IFN-β concentration evolved according to the stochastic input from IFN-β secreting cells and removal of the cytokine due to cellular uptake and extracellular degradation. IFN-β was always detectable in the supernatants of the cultures, indicating high molecule number. Therefore, the IFN-β concentration was updated in parallel with the Gillespie steps using a (deterministic) explicit Euler method. Because of the high diffusion coefficient of IFN (Kreuz & Levy, 1965), the extracellular diffusion of IFN is fast (minutes for N of the order 100) when compared to the timescale of IFN expression and response (several hours). Accordingly, we assumed uniform distribution of secreted IFN.

Depending on the applied virus titer, we consider a fraction of cells as infected (Figure 2A). Of these cells, a certain percentage will eventually express IFN-β, according to the measured fraction of IFN-β-tGFP$^+$ cells (Figures 1C, 2A). As the MOIs used in the experiments are approximately unity or below, the number of infecting viral particles per cell is low; each of the infected cells was randomly assigned a viral load of 1-3 virus particles. To execute a time step of the dynamics, we considered all possible state changes of the cells in the system and chose a time step dt and the state change to be realized according to Gillespie's direct method. To obtain a compact computational description of the system that can be compared with the live-cell imaging data, we chose phenomenological propensity functions w as follows:

(1) Let V_i denote the virus number in cell i. The rate of virus replication is

$$w^+_{\mathrm{V},i} = r\, V_i\, \delta,$$

where r denotes the rate constant of virus replication, and the function

$$\delta = \begin{cases} 1 & \text{if } V_i < V_{\max} \\ 0 & \text{if } V_i \geq V_{\max}, \end{cases}$$

was chosen to account for a limited capacity of an intact cell to harbour $V_{\max}$ viral particles.

(2) Virus activates the RIG-I pathway with transition rate

$$w^+_{\mathrm{R},i} = k_{\text{RIG-I}} \frac{V_i^{h_\mathrm{V}}}{K_\mathrm{V}^{h_\mathrm{V}} + V_i^{h_\mathrm{V}}},$$

implementing saturation with respect to viral particle number and allowing for a threshold response of the RIG-I pathway. In addition, we model inactivation of the RIG-I pathway (including re-accumulation of the transcription factors in the cytoplasm) with rate

$$w^-_{\mathrm{R},i} = l_{\mathrm{RIG\text{-}I}}.$$

(3) After nuclear translocation of NF-κB and IRFs, the IFN-β gene is induced with rate

$$w^+_{\mathrm{I},i} = k_{\mathrm{IFN}}.$$

and terminated with

$$w^-_{\mathrm{I},i} = l_{\mathrm{IFN}}.$$

(4) IFN-producing cells secrete IFN-β with rate k_{S}, and extracellular IFN-β I is degraded with rate constant d_{IFN}.

(5) Extracellular IFN-β I binds to the IFNAR and activates STAT1 and STAT2 with rate

$$w^+_{\mathrm{STAT},i} = k_{\mathrm{STAT}} \frac{I^{h_{\mathrm{IFN}}}}{K_{\mathrm{IFN}}^{h_{\mathrm{IFN}}} + I^{h_{\mathrm{IFN}}}},$$

where k_{STAT}, K_{IFN} and h_{IFN} denote maximal rate, the half-saturation constant and the Hill coefficient, respectively.

(6) Activated STAT1/2 mediate the expression of ISGs, including IRF-7 whose induction we have imaged. IRF-7 is induced with rate

$$w^+_{\mathrm{ISG},i} = k_{\mathrm{ISG}}.$$

As there is considerable time delay between the induction of IFN-β by virus and IRF-7 by the secreted IFN (Figure 6C; IRF-7 producers are half-maximal when IFN-β producers have already plateaued), we have not implemented positive feedback of IFN-β on IFN-β induction via upregulation of IRF-7. The comparative unimportance of this feedback loop in our system was confirmed by simulating a version of the model with feedback (with $w^+_{\mathrm{I},i}$ being dependent on the IRF-7 level in the cell) that gave essentially the same results as the model version without feedback used in the paper.

(7) In cells that express ISGs, we assume that further viral replication is inhibited and viral load declines with the rate

$$w^-_{\mathrm{V},i} = d V_i.$$

An additional mechanism for accounting for the observed overall decrease of viral load after its peak at ~18 h (Figure 6C) is the death of virus-infected cells. For simplicity, we have neglected this effect in the model. To keep the model as simple as possible, we neglected also cell

proliferation, thus simulating a non-growing cell population. This approximation is justified by the fact that we did not observe obvious differences in heterogeneous IFN-β induction between the cell fraction dividing during the time of observation (Figure 4A) and the entire cell population that contains a sizable fraction of non-dividing cells (Figure 3C).

The coupled stochastic simulations for the cell states and the deterministic iteration of extracellular IFN-β concentration were performed as follows. First we computed the time interval dt after which the next stochastic switching event occurs, according to

$$\mathrm{d}t = - \frac{\log(r_1)}{\sum_i w_{\cdot,i}},$$

where $\sum_i w_{\cdot,i}$ extends over all propensities that 'lead away' from the current state of the system and r_1 is an uniformly distributed random number. A second random number r_2 is then used to draw the state transition actually occurring. Note that in this algorithm, there is no need to randomly pick cells in which the transition occurs. The extracellular IFN-β concentration I is updated as follows:

$$I(t+dt) = I(t) + \left[\mathrm{d}t \; k_S \; N_P(t) \; - d_{IFN} \; I(t)\right],$$

where $N_P(t)$ is the number of IFN-β expressing cells at time t. This is of course the discrete Euler approximation of the differential equation $\mathrm{d}I/\mathrm{d}t = k_S \; N_P(t) - d_{IFN} \; I(t)$ provided that the time step dt is sufficiently small: $\mathrm{d}t << d_{IFN}^{-1}$. We found the latter condition to be guaranteed with the parameter choices for the model. As IFN-β diffuses rapidly compared with the typical time scale of the model dynamics of hours, spatial gradients of I(t) were neglected.

To compare the model with the experimental data, we used the following readouts (Figure 6C):

- The total viral load of the cell population is updated by

$$V(t) = \sum_{i=1}^{N} V_i(t),$$

  where we used an appropriate scaling factor to relate virus particles (in the model) to the mean fluorescence intensity of the HN staining (in the experiment).
- The fraction of IFN-β-positive cells.
- The extracellular IFN concentration $I(t)$.
- The fraction of ISG-expressing cells, corresponding to the cells with expression of IRF-7-mCherry reporter.

2. Parameter estimation

We found that the simulation time of the full model for a sufficiently large number of cells (10^4) of several hours is prohibitive of straightforward optimization approaches for parameter estimation. Therefore we divided the parameter estimation problem into three parts: (i) Determination of parameters for IRF/NF-κB activation, (ii) Determination of the parameters of IFN-β expression and (iii) Determination of parameters for STAT1/2 activation and ISG expression. For the first two parts, coupling between the cells via secreted IFN-β can be neglected, as in our model there is no autocrine/paracrine feedback to IFN-β expression (Ulfert Rand, unpublished data). The absence of paracrine coupling means that IRF/NF-κB transcription factor activation and IFN-β induction can be simulated much faster than the complete model and is amenable to rigorous parameter estimation. For the third part, ISG induction, paracrine coupling is relevant, implying the need for simulating large numbers of cells and thus having impractically long simulation times for parameter estimation. However, it turns out that we can still infer salient quantitative features of ISG expression from the experimental data.

2.1 NF-κB/IRF activation

NF-κB/IRF-7 nuclear translocation and the IFN-β expression have been imaged in single cells, yielding distributions for the nuclear translocation times of the transcription factors and the onset of IFN-β-tGFP expression (Figure 3E, Supplementary Figure S10A and C, respectively). As these "passage time" represent an up to now unique data set, we focused the parameter estimation on reproducing these distributions with the model. Several mechanistically relevant conclusions will be drawn from these calculations, as discussed at the end of this subsection.

We begin by estimating the parameters of the transition rates for NF-κB/IRF-7 nuclear translocation induced by RIG-I signalling, $w^{+}_{\mathrm{R},i}$. The distribution of NF-κB/IRF-7 translocation times can be computed by simulating a submodel of viral replication and subsequent NF-κB/IRF-7 activation using Gillespie's algorithm. First, we sought a satisfactory match of the model with the measured time course of viral replication at 40 HAU/ml. This was achieved by setting the viral replication parameters r, $V_{\max}$ and d to the values given in Supplementary Table S1 (for the match of model and data, see Figure 6D, upper trace).

Next, we computed the distribution of NF-κB/IRF translocation times by simulating the submodel sufficiently often ($5\mathrm{x}10^4$ runs). To match this computed distribution with the measured one, we allowed the parameters of the RIG-I pathway (activation rate constant $k_{\text{RIG-I}}$, half-saturation constant for activation by virus K_{V}, and Hill coefficient for activation by virus h_{V}) to vary while keeping the previously determined viral replication parameters fixed. As objective function, we used the squared distance of the binned experimental and simulated data:

$$\chi^2_{\text{Neyman}} = \sum_{i=1}^{B} \frac{(\mathrm{D}_i - \mathrm{E}_i)^2}{\mathrm{D}_i},$$

where B, D_i and E_i denote the number of bins of the histograms, the number of observed events in the ith bin and the number of simulated events in the ith bin, respectively, under the condition

$$\sum_{i=1}^{B} \mathrm{D}_i \quad = \quad \sum_{i=1}^{B} \mathrm{E}_i .$$

Following Neyman (Baker & Cousins, 1984), the measurement error for each bin is estimated according to the number of observed events, $\mathrm{CV}_i = 1/\sqrt{\mathrm{D}_i}$, yielding the denominator D_i in the χ^2_{Neyman} function.

For accuracy, we chose a much larger number of simulation runs ($5\mathrm{x}10^4$) than experimentally observed cells (315). We used the cumulative distribution function (cdf) of the simulations and calculated the number of simulated events in the *i*th bin as follows:

$$\mathrm{E}_i \quad = \quad N_{\mathrm{Data}} \left(\mathrm{cdf}(t^i_{j+1}) - \mathrm{cdf}(t^i_j)\right),$$

where N_{Data} denotes the number of observed data points, and t^i_j and t^i_{j+1} are the left and the right bin edge of the *i*th bin, respectively.

We employed simulated annealing to minimize the objective function χ^2_{Neyman}. The resulting parameter values ($k_{\mathrm{RIG\text{-}I}}$ = 0.48/h, h_{V} = 3.0, K_{V} = 43 and $l_{\mathrm{RIG\text{-}I}}$ = 0.4/h) yield a very good match of computed and measured distributions of nuclear translocation times of the transcription factors (Supplementary Figure S10A).

Arguably the most interesting feature of this parameter set in biological terms is the high Hill coefficient h_{V}, implying cooperative activation of the RIG-I pathway by virus. To establish how robust this estimate is, we used the profile-likelihood method (Venzon & Moolgavkar, 1988; Raue et al, 2009). We fixed h_{V} systematically to different values around the estimated optimum of h_{V} = 3.0 and refitted $k_{\mathrm{RIG\text{-}I}}$, $l_{\mathrm{RIG\text{-}I}}$ and K_{V} by simulated annealing. Supplementary Figure S10B shows for each h_{V} the χ^2_{Neyman} obtained after optimization of $k_{\mathrm{RIG\text{-}I}}$ and K_{V}. This profile likelihood shows that non-cooperative activation of the RIG-I pathway (h_{V} = 1) results in a significantly worse fit of the translocation-time distribution. It far exceeds the degrees of freedom (df = B – 1 – # fit parameters = 8), showing that the fit is extremely poor when the measurement error in the data is considered. By contrast, $h_{\mathrm{V}} \geq 3$ yields indistinguishably good fits. This we conclude that activation of the RIG-I pathway by virus is cooperative, while the available data are insufficient to estimate the precise degree of cooperativity.

2.2 IFN-β expression

After nuclear translocation of the transcription factors NF-κB and IRF-3/7 most of the cells (91% at 80 HAU/ml NDV) induce the IFN-β gene with variable time delay T_{gen} (Figure 3E). The observed cell-to-cell variation of this time delay results in a distribution of IFN-β induction times after transcription factor activation (Supplementary Figure S10C).

For the following arguments, we recall that for the present stochastic modelling of *Ifnb* promoter activation after nuclear translocation of NF-κB and IRFs, the Markov property must be fulfilled. The latter requires that the state change of the system depend only on the current state. Since the exponential distribution is the only continuous distribution without memory, the individual transition rates in a Markov model are distributed exponentially.

The observed distribution of T_{gen} obviously cannot be described by a single exponential distribution (Supplementary Figure 10C). Instead, there is a distinct time delay between transcription factor translocation and IFN-β induction (note that the distribution of transcription factor translocation times can neither be modelled by a single exponential, cf. Supplementary Figure S10A; here the time delay is due to viral replication, see Section 2.1 of this supplement). *Ifnb* gene activation is a multi-step process (Ford and Thanos 2010), and this will generate time delay. Therefore we analysed if the T_{gen} histogram can be fitted with a Gamma distribution $\gamma(m,\lambda)$, which describes the sum of m independent and with parameter λ exponentially distributed random numbers. The density function of the gamma distribution f_γ is

$$f_\gamma(t) = \begin{cases} \frac{\lambda^m}{\Gamma(m)} t^{m-1} \mathrm{e}^{-\lambda t} & t \geq 0 \\ 0 & t < 0, \end{cases}$$

where m and λ term positive parameters and $\Gamma(m)$ denotes the gamma function

$$\Gamma(m) = \int_0^\infty t^{m-1} e^{-t}\, dt.$$

We used the maximum-likelihood method to estimate the parameters of the gamma distribution $\gamma(m,\lambda)$. To this end, we analysed the maximum of the log-likelihood function of the gamma distribution

$$\begin{aligned} \mathcal{L}(m,\lambda,t_i) &= \log\left(L(m,\lambda,t_i)\right) \\ &= \log\Big(\prod_{i=1}^{N_{\mathrm{Data}}} \frac{\lambda^m}{\Gamma(m)} t_i^{m-1} \mathrm{e}^{-\lambda t_i}\Big) \\ &= N_{\mathrm{Data}} \log\Big(\frac{\lambda^m}{\Gamma(m)}\Big) + \sum_{i=1}^{N_{Data}} \log\left(t_i^{m-1} \mathrm{e}^{-\lambda t_i}\right), \end{aligned}$$

where N_{Data} terms the number of observed data points of T_{gen}. The root of the partial derivative of the log-likelihood with respect to λ yields a direct estimator for λ:

$$\begin{aligned} \frac{\partial \mathcal{L}(m,\lambda,t_i)}{\partial \lambda} &\overset{!}{=} 0 \\ \Leftrightarrow \qquad \lambda &= \left(\left(\frac{1}{N_{\mathrm{Data}}\, m}\right) \sum_{i=1}^{N_{\mathrm{Data}}} t_i\right)^{-1}. \end{aligned}$$

Similarly, we obtain an implicit estimate of m:

$$\frac{\partial \mathcal{L}(m,\lambda,t_i)}{\partial m} \stackrel{!}{=} 0$$

$$\Leftrightarrow \underbrace{\log\left(N_{\text{Data}}\, m\right) - \log\left(\sum_{i=1}^{N_{\text{Data}}} t_i\right) - \frac{\Gamma'(m)}{\Gamma(m)} + \frac{1}{N_{\text{Data}}} \sum_{i=1}^{N_{\text{Data}}} \log(t_i)}_{=:\ \mathcal{M}(m,t_i)} \stackrel{!}{=} 0.$$

Note that the determination of m is independent of computing λ. Using the observed data points of T_{gen}, we obtain m = 6.4. In the following, we interpret m as the number of exponentially distributed steps in a stochastic process. Hence we set m to the nearest integer, m = 6. In turn, this yields λ = 1.79/h. Thus the T_{gen} can be well approximated by six consecutive exponentially distributed steps with half-life ln 2/λ = 23 min (Supplementary Figure S10C). We note that the estimated number of steps and half-life corresponds well with the mechanistic knowledge about the formation of the *Ifnb* enhanceosome (Ford and Thanos, 2010), although transcription and translation might also contribute relevant steps.

Besides, we have observed an average duration of IFN expression in individual cells with time of ~13 h. Accordingly, IFN-β expression is terminated with

$$w_{\text{I},i}^{-} = l_{\text{IFN}},$$

where l_{IFN} = 0.08/h.

2.3 ISG induction

To obtain quantitative insight into IRF-7 regulation by secreted IFN-β and apply this for the parameterization of the model, we used the data in Figure 5A to compute the dose response of the fraction of IRF-7-expressing cells as a function of extracellular IFN-β concentration I. The hyperbolic function

$$\text{Fraction of IRF-7-expressing cells} = \frac{I}{K_{\text{IFN}} + I}$$

provides an excellent fit to the data, with K_{IFN} = 100.89 U/ml (Supplementary Figure S10D). Therefore, IRF-7 induction is non-cooperative, fixing also h_{IFN} = 1.

In contrast to the dose-response parameters K_{IFN} and h_{IFN}, the rate constants for STAT1/2 activation and ISG induction cannot be rigorously fitted from the available data. We found that for k_{STAT} = k_{ISG} = 0.1/h, the computed time course of ISG expression agreed with the experimentally measured one at high viral load (Figure 6D, lowest panel; 40 HAU/ml NDV).

Within the simulation time of 48 h the number of IRF-7 expressing cells remained high (Figure 6C). Hence we set the rate for termination of ISG expression and STAT1/2 activation to zero:

$$w^{-}_{\mathrm{ISG},i} = w^{-}_{\mathrm{STAT},i} = 0.$$

Finally, we note that the IFN-β secretion rate per cell has been estimated simply by comparing the kinetics of the IFN-β-producing cell fraction and the appearance of IFN-β in the supernatant. Setting k_S = 0.13 U/ml per hour per cell and d_{IFN} = 0.15/h yielded good agreement with the experimental data (Figure 6D; second and third panel).

References

Baker S, Cousins RD (1984) Clarification of the use of chi-square and likelihood functions in fits to histograms. *Nuclear Instruments and Methods in Physics Research* **221:** 437-442

Kreuz LE, Levy AH (1965) Physical Properties of Chick Interferon. *J Bacteriol* **89:** 462-469

Raue A, Kreutz C, Maiwald T, Bachmann J, Schilling M, Klingmüller U, Timmer J (2009) Structural and practical identifiability analysis of partially observed dynamical models by exploiting the profile likelihood. *Bioinformatics* **25:** 1923-1929

Venzon DJ, Moolgavkar SH (1988) A Method for Computing Profile-Likelihood-Based Confidence Intervals. *Applied Statistics* **37:** 87-94